ACS Photonics

Article

pubs.acs.org/journal/apchd5

Plasmonic Bulk Heterojunction Solar Cells: The Role of Nanoparticle Ligand Coating

Emmanuel Kymakis,[†] George D. Spyropoulos,[†,‡] Rute Fernandes,[§] George Kakavelakis,[†,‡] Antonios G. Kanaras,[§] and Emmanuel Stratakis*[,†,‡,⊥]

[†]Center of Materials Technology & Photonics and Electrical Engineering Department, School of Engineering, Technological Educational Institute (TEI) of Crete, Heraklion, 71004 Crete, Greece

[‡]Department of Materials Science and Technology, University of Crete, Heraklion, 71003 Crete, Greece

[§]Physics and Astronomy, Faculty of Physical Sciences and Engineering, University of Southampton, Southampton, SO171BJ, United Kingdom

[⊥]Institute of Electronic Structure and Laser (IESL), Foundation for Research and Technology-Hellas (FORTH), Heraklion, 711 10 Crete, Greece

Supporting Information

ABSTRACT: There has been a lot of interest regarding the influence of active-layer-incorporated plasmonic nanoparticles (NPs) in the performance of bulk heterojunction organic photovoltaic (OPV) devices, while both an increase and decrease in performance have been reported. In this paper, following a systematic approach, we demonstrate strong evidence of the critical importance of the NPs' ligand shell on the device performance. In particular, it is argued that the plasmonic effect accountable for the performance enhancement takes place only in the case in which the NP's core is in direct contact with the active layer polymer donor. This can be achieved with the utilization of either ligand-free NPs or NPs terminated with the same polymer donor as the active layer. Using this concept we achieved an enhanced efficiency of 7.16% in OPV devices incorporating the poly(3-hexylthiophene-2,5-diyl) (P3HT):indene-C60 bisadduct (ICBA) active layer. On the contrary, devices with ligand-terminated Au NPs show lower performance, even compared with the reference, NP-free, device due to the deteriorated active layer morphology attained, which leads to exciton quenching. These new insights into the plasmonic light-harvesting technology could shed light on the existing controversy and provide guidelines for device design and fabrication.

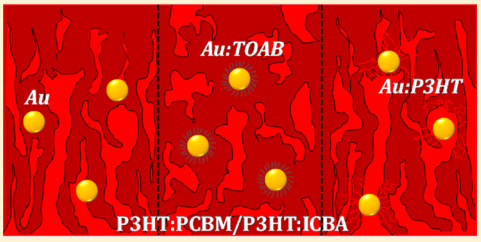

KEYWORDS: *organic solar cells, bulk heterojunction, plasmonic nanoparticles, ligand coating*

Organic solar cells are strong candidates for the development of cost-effective, lightweight solar energy conversion. A major advantage of this technology is the ability to manipulate the concentration and functionality of the components within the active layer, which in return allows the tuning of the device optoelectronic characteristics. Currently, the most efficient single-junction OPV device exhibits power conversion efficiencies (PCEs) of over 9% and is based on a polymer−fullerene bulk heterojunction (BHJ) active layer architecture, characterized by a complex interpenetrating network of two polymer phases.[1,2] Organic photovoltaic (OPV) commercialization is expected to spark once the efficiencies for single-junction devices exceed 10%.[3−5] A major barrier against further improvement of OPVs is the fundamental trade-off between efficient light absorption (which requires a thick device) and efficient photogenerated carrier collection (which requires a thin device).[6] Indeed, charge transport in BHJ OPVs is accomplished provided that continuous pathways for both types of carriers exist, but the presence of such pathways is less likely for thick active layers. This drawback poses limitations on the thickness of the active layer, which, usually, should not exceed 200 nm.[7]

Thus, one of the major challenges in the field is to develop new strategies aiming for the enhancement of light absorption, which can result in a higher number of excitons generated. Recent research indicates that a fascinating strategy to increase the number of excitons is by "trapping" incident light into the active layer by means of metallic nanoparticles (NPs).[8,9] Plasmonic NPs are known to exhibit a strong absorption band in the UV−visible region, due to excitation of localized surface plasmon resonance (LSPR) modes (LSPR, nonpropagating excitations of conduction electrons within a metallic nanostructure), which lie within the optical absorption band of the conjugated polymers used in the active layer. The enhanced plasmonic optical field at the vicinity of NPs is coupled to the photoactive layer, increasing its effective absorption cross-section and thus exciton yield.[10,11]

Received: February 9, 2015
Published: May 6, 2015

DOI: 10.1021/acsphotonics.5b00202
ACS Photonics 2015, 2, 714−723

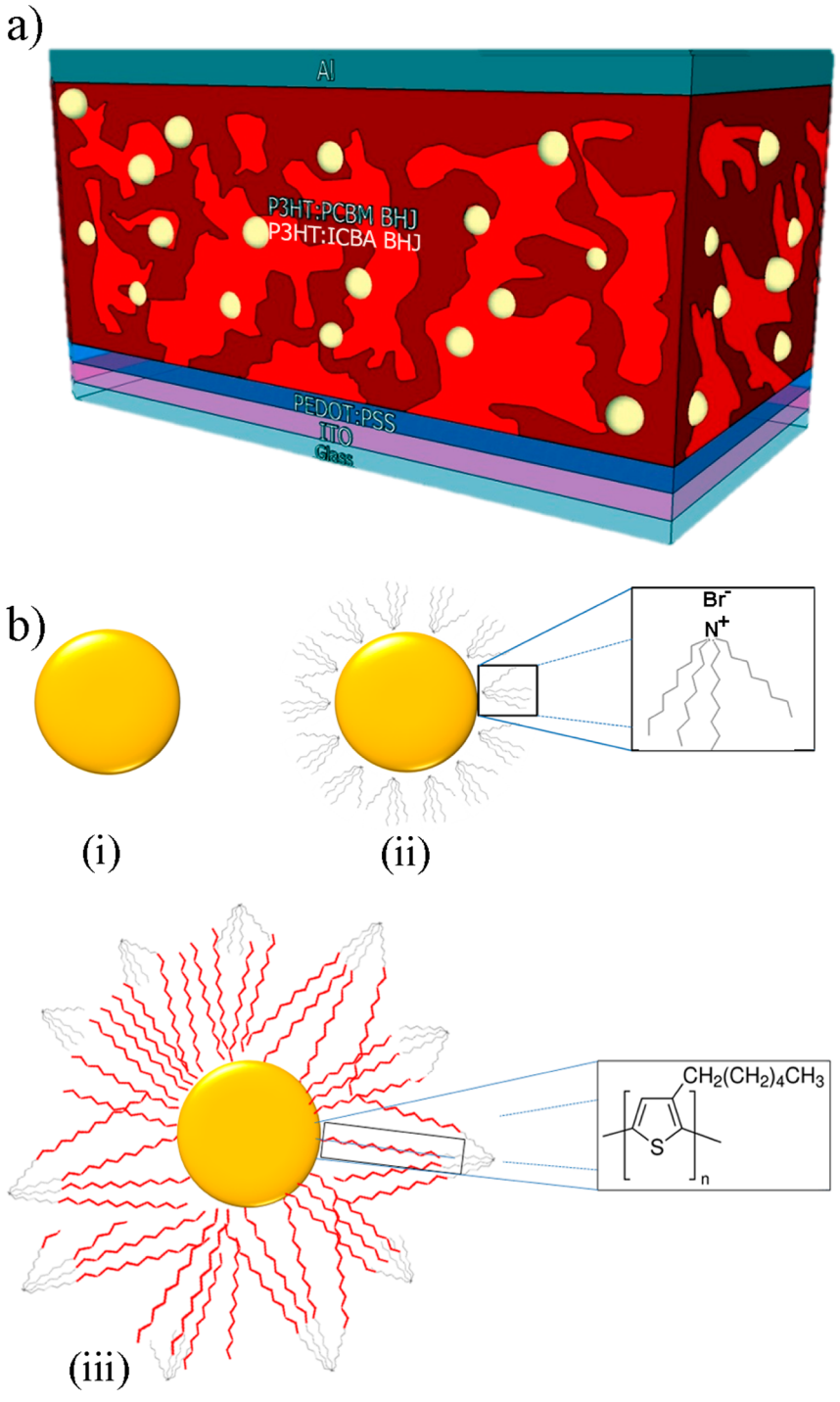

Figure 1. (a) Schematic representation of the BHJ OPV cell architecture; (b) the three types of NPs embedded into the active layer, namely, bare (i), TOAB-terminated (ii), and P3HT-terminated (iii).

However, recent studies concerning the effect of NP incorporation into the active layer are rather controversial. There are several groups discussing that the PCE slightly increases upon dispersion of plasmonic NPs into the active layer,[12−16] while others report that PCE decreases.[17,18] Besides this, it was reported that the addition of chemically synthesized plasmonic NPs in the active layer not only enhances the local absorption of light but also leads to increased carrier recombination.[17] This effect was recently verified using a combination of ultrafast optical spectroscopy and electrical characterization measurements.[19] In this context, we have previously suggested that the presence of a ligand coating on the NPs may promote undesirable exciton quenching, via nonradiative energy transfer between the NPs and the active layer.[14] To support this hypothesis, metallic NPs formed by a physical laser ablation method[20,21] that are free of surfactants were used as additives. It was demonstrated that the device performance can be significantly enhanced by 40%. The effect was attributed to LSPR and blend morphology effects,[22,23] but no concrete conclusion was drawn on the mechanism responsible for the remarkable improvement of device performance.

DOI: 10.1021/acsphotonics.5b00202
ACS Photonics 2015, 2, 714−723

This work sheds light on the important role of the NPs' ligand shell on the performance of BHJ OPV devices. In a systematic study, Au NPs of different ligand coatings are deliberately employed and the variations in device characteristics are carefully analyzed. Our studies reveal that the best PCE is obtained for poly(3-hexylthiophene-2,5-diyl) (P3HT) mixed with fullerene acceptor derivative (phenyl-C61-butyric acid methyl ester (PCBM) and indene-C60 bisadduct (ICBA)) cells doped with NPs terminated with P3HT chains. On the other hand, the significant inferior performance of devices doped with ligand-encapsulated NPs can be attributed to the deterioration of the active layer morphology attained.

RESULTS AND DISCUSSION

All the experiments were performed using the P3HT as electron donor material since one of the ligands used in this work was P3HT polymer, and the well-studied PCBM fullerene derivative was used as electron acceptor material in the case of air-processed OPVs and an ICBA fullerene derivative with optimized energy levels (shifted lowest unoccupied molecular orbital by 0.17 eV toward the vacuum level) in the case of highly efficient OPVs processed under an inert atmosphere. Since the P3HT:PCBM BHJ system is the best characterized OPV system, the conditions for optimum performance are well identified, but more importantly it is a highly reproducible system that enables a quantitative study of the effect of the NPs' ligand shell on the photovoltaic performance. The P3HT:ICBA BHJ system[24] was used to validate our findings for the case of high-efficiency OPV cells as well. Initially, gold nanoparticles synthesized by the Brust method[25] and coated with tetraoctyl ammonium bromide (Au:TOAB) were incorporated in both BHJ systems as light-harvesting components. In such polymer–nanoparticle blends, although the light absorption was monotonically increased with incorporating increasing amounts of metal NPs into the active layer, at the same time the short-circuit current (J_{sc}), open-circuit voltage (V_{oc}), and fill factor (FF) of the ensuing devices monotonically decreased (results not shown). The observed decrease can be attributed to the NPs acting as recombination centers within the device, in essence creating internal short circuits throughout the photoactive layer. This adverse effect of NP-assisted recombination had also been confirmed experimentally by Wu et al., via transient absorption spectroscopy measurements.[19]

To further examine the influence of plasmonic NPs on OPV device performance and clarify the observed Au:TOAB NPs' deterioration effect, incorporation of two additional NP types was investigated: (a) surfactant-free, ion-terminated Au NPs prepared by physical synthetic means[21] and (b) P3HT-terminated Au NPs (Au:P3HT). Both NP types (made chemically and by ablation) exhibit similar size distributions (Supporting Information). Practically both systems allow direct contact of NPs with the active layer components and potentially improved exploitation of the plasmon absorption enhancement process.[26] At the same time, the different termination coatings among the three types of NPs used enable the investigation of the effect of ligand molecules on plasmonic enhancement.

Figure 1 presents a schematic of the different OPV cell setups discussed in this work. These cells are based on the configuration ITO/PEDOT:PSS/P3HT:fullerene/interlayer-(optional)/Al with three different types of Au NPs embedded into the active layer. The corresponding UV–vis absorption spectra of the optimized P3HT:PCBM-based devices in each case are shown in Figure 2a. The red shoulder at 602 nm indicates the effective self-organization of the regioregular P3HT. In the spectral region between 450 and 650 nm where the P3HT:PCBM absorbs, an increase in the percentage of absorbance occurred for all NP-based OPVs. Figure 2b presents the respective absorption enhancement (ratios of the

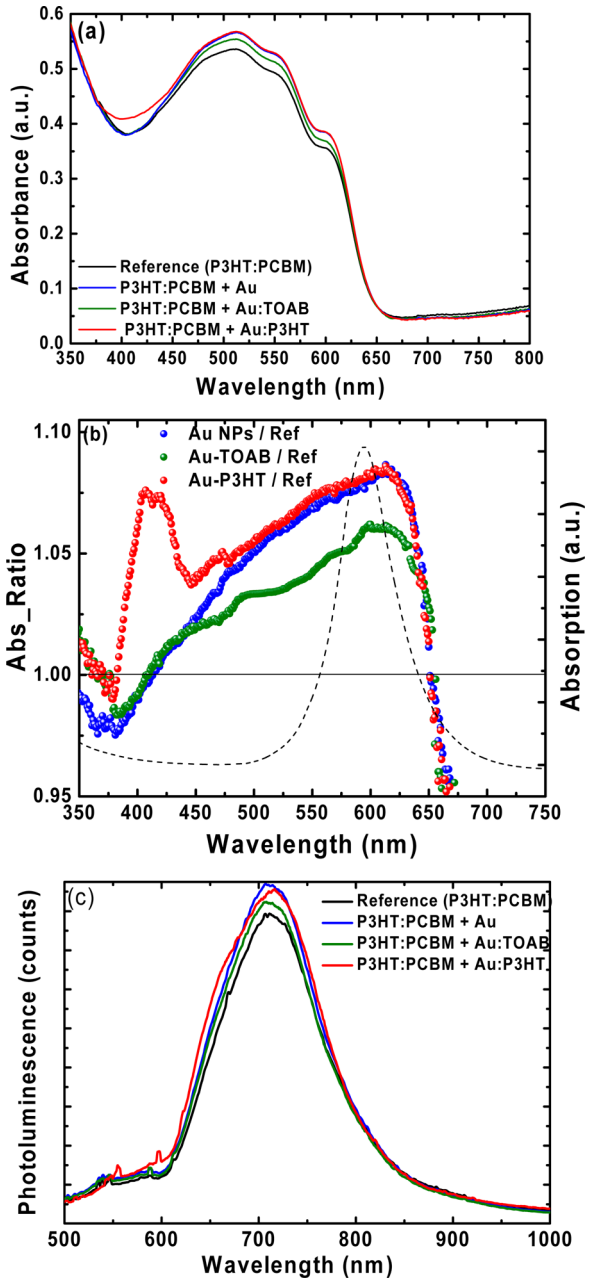

Figure 2. (a) Absorption spectra of the BHJ OPV devices with different types of Au NPs embedded into the active layer (the absorbance is baseline corrected with the PEDOT:PSS/ITO/glass substrate as a reference). (b) Absorption enhancement factor of the devices (relative ratios of the absorption spectra of NP-embedded devices to that of the pristine one). The calculated extinction spectrum of Au NPs embedded in the P3HT:PCBM medium is plotted for comparison (dashed line). The dielectric constants of P3HT:PCBM were obtained from ref 28. (c) Normalized PL spectra of reference and P3HT:PCBM active layers blended with different types of Au NPs. Each spectrum is normalized by the respective active layer absorption at the excitation wavelength.

DOI: 10.1021/acsphotonics.5b00202
ACS Photonics 2015, 2, 714–723

absorption spectra of the Au NP-based devices to that of the pristine one), together with the extinction (scattering plus absorption) spectra for 8 nm Au NPs embedded in P3HT:PCBM media, as calculated using Mie theory.[27] For the calculation of these extinction spectra the optical constants of P3HT:PCBM were used,[28] leading to a red-shift of the resonance peak with respect to that recorded in ethanol. Notably, the absorption enhancement for bare as well as Au:P3HT NP-doped devices exhibits a maximum at 610 nm, which fairly coincides with the extinction peak of the Au NPs, indicating that absorption improvement is due to the LSPR effect. The long tail to the absorption enhancement curves toward lower wavelengths suggests efficient scattering from larger diameter Au NP aggregates formed during the spin-coating process.[29] On the contrary, for the Au:TOAB-doped devices the absorption enhancement is lower and the LSPR effect is weaker; this is probably due to the adverse effect of the TOAB ligand, which acts like an optical spacer between the NPs and polymer absorber, giving rise to a decreased plasmon optical field at the donor chains in the vicinity of NPs.

The photoluminescence (PL) spectra of the P3HT:PCBM-based devices with Au NPs embedded in the active layer in various concentrations are shown in Figure 2c. In all cases, the incorporation of Au NPs leads to broader PL spectra and an increase of the PL. Such enhancement can be attributed to the fact that the LSPR excitation increases the degree of light absorption and, thereby, enhances the exciton generation rate.[30] Moreover, the enhanced PL intensity can arise from the strong coupling between the excitonic state of P3HT and the plasmonic field of the NPs, which is due to the propagating oscillation of the surface plasmon dipole plasmonic field and excitons.[31]

To verify that the enhancements presented in Figure 2 are a fair representation of the light absorbed into the active layer and subsequent exciton generation, we have fabricated a series of OPV devices. Figure 3a shows the current−voltage (J−V) characteristics for a series of eight different cells in each case for the P3HT:PCBM photoactive blend. The respective averaged photovoltaic characteristics are summarized in Table 1. It is observed that the incorporation of Au:P3HT NPs in both active layers induces a significant improvement of both the device short-circuit current (J_{sc}) and the fill factor (FF), whereas the open-circuit voltage (V_{oc}) remains constant. As a result, a 37.2% increase in PCE is obtained compared to the reference device. The situation is similar to the case of devices doped with ablated Au NPs, where a 20.3% increase in PCE is attained. On the contrary, the Au:TOAB-doped devices exhibited inferior performance compared to either of the above cases as well as to the reference device. It is important to note that the above results did not qualitatively change when the efficiency of OPV devices was further improved upon using a bilayer Ca/Al cathode (ITO/PEDOT:PSS/P3HT:PCBM/Ca/Al). The respective J−V and photovoltaic characteristics are presented in Figure S2 and Table S2.

In order to investigate the underlying mechanism responsible for the enhanced performance of the devices, the incident photon-to-electron conversion efficiency (IPCE) curves of the respective devices were recorded (Figure 4a). The corresponding increase in IPCE (ΔIPCE) is presented in Figure 4c. It can be observed that IPCE increases considerably upon the incorporation of bare and Au:P3HT NPs, which complies with the enhanced J_{sc} observed in both cases, indicating photocurrent generation from light harvested by the NPs. In

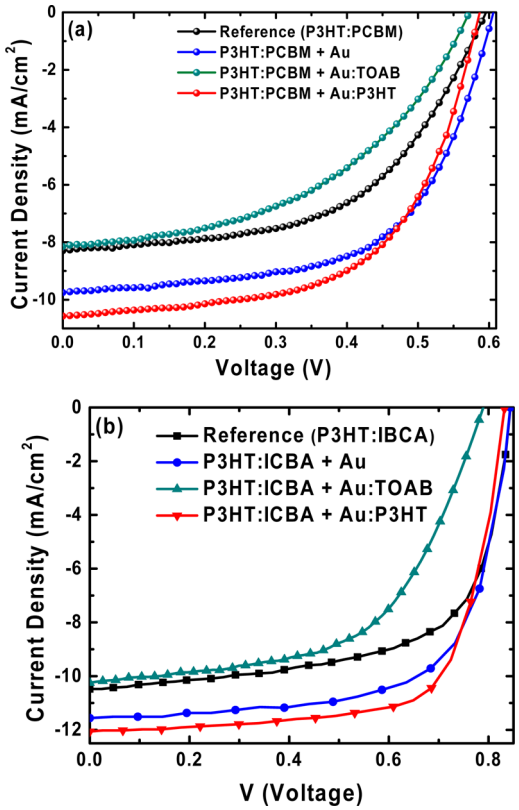

Figure 3. J−V characteristics of reference and OPV devices of the configuration (a) ITO/PEDOT:PSS/P3HT:PCBM/Al and (b) ITO/PEDOT:PSS/P3HT:ICBA/Ca/Al incorporating different types of Au NPs into the active layer.

particular, the IPCE of both types of devices becomes enhanced in a broad spectral range (480 to 700 nm), while it maximizes at 580 nm. This wavelength regime practically coincides with the spectral range in which the optical absorption of the Au NPs embedded in P3HT:PCBM medium is enhanced due to the LSPR effect (Figure 2b). On the contrary in the Au:TOAB-doped devices, although an absorption enhancement factor was obtained (Figure 2b), IPCE decreases compared to the reference cell. Considering that ΔIPCE for bare and Au:P3HT NPs becomes maximum close to the plasmon absorption peak, IPCE enhancement can be attributed to the local enhancement of the incident electromagnetic irradiation field in the vicinity of small-sized NPs, due to LSPR effects. On the other hand, as our group recently showed by means of combined X-ray reflectivity and AFM measurements, the incorporation of surfactant-free NPs in the photoactive layer also gives rise to enhanced structural stability of the blend and, therefore, optimized blend morphology,[32,33] an effect that explains the observed disparity between the absorption and the IPCE enhancement. In this context we postulate that the reason for the substantially decreased IPCE observed for Au:TOAB NPs, despite the absorption enhancement shown in Figure 2b, may be due to the deterioration of the active layer morphology, as a result of the interaction of the TOAB surfactant molecules with the active polymer chains. This further suggests that in the presence of P3HT ligands the blend morphology is not disturbed.

In a first attempt to investigate the effect of NPs' ligand shell on active layer morphology, atomic force microscopy (AFM) studies of the surfaces of the different blends were conducted.

DOI: 10.1021/acsphotonics.5b00202
ACS Photonics 2015, 2, 714−723

Table 1. Photovoltaic Characteristics of Solar Cells of the Configuration ITO/PEDOT:PSS/P3HT:PCBM/Al, Incorporating Different Types of Au NPs into the Photoactive P3HT:PCBM Layer

active layer	J_{sc} (mA/cm^2)	V_{oc} (V)	FF (%)	PCE (%)	μ_h (cm^2/(V s))
P3HT:PCBM	8.30 ± 0.12	0.60 ± 0.02	53.83 ± 0.30	2.66 ± 0.05	8.98×10^{-4}
P3HT:PCBM + Au	9.45 ± 0.21	0.60 ± 0.03	56.65 ± 0.32	3.20 ± 0.09	1.17×10^{-3}
P3HT:PCBM + Au:TOAB	8.15 ± 0.11	0.57 ± 0.03	46.74 ± 0.21	2.18 ± 0.04	7.83×10^{-4}
P3HT:PCBM + Au:P3HT	10.54 ± 0.26	0.59 ± 0.02	58.90 ± 0.34	3.65 ± 0.11	1.26×10^{-3}

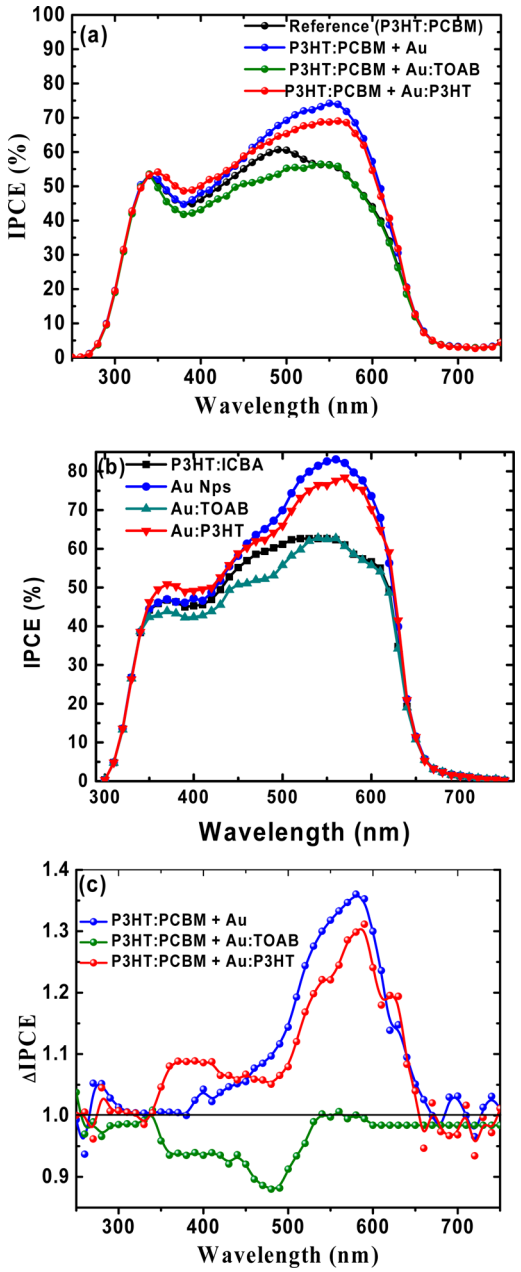

Figure 4. IPCE curves of reference and OPV devices incorporating different types of Au NPs into the P3HT:PCBM (a) and P3HT:ICBA (b) active layers, respectively. (c) ΔIPCE curves (relative ratios of the IPCE spectra of NP-embedded devices to that of the pristine one) of the P3HT:PCBM-based plasmonic devices.

As shown in Figure 5, the BHJ layer of the best OPV devices showed increased roughness compared to the reference and Au:TOAB NP-doped ones. Besides this, the Au:P3HT NP-doped blend showed a much coarser texture with broad hill-like features, compared to the other BHJ layers. It has been suggested that a rough P3HT:PCBM surface indicates enhancement of the ordered structure that assists exciton dissociation.[34] Moreover, it has been reported that an increase of blend roughness will give rise to a corresponding increase of the interface area between the anode and the active layer, providing shorter routes for holes to travel to the anode and thus enhancing hole mobility.[34,35] To test this in our case, hole-only devices were fabricated for all different types of devices. As shown in Table 1, the hole mobilities of the reference device as well as those blended with surfactant-free Au, Au:TOAB, and Au:P3HT NPs are calculated from the currents in the square law region to be 8.98×10^{-4}, 1.17×10^{-3}, 7.83×10^{-4}, and 1.26×10^{-3} cm^2 V^{-1} s^{-1}, respectively. Therefore, it is clear that the hole mobility decreases for the Au:TOAB NP-doped cells due to inferior hole transport. Finally, the reduced mean distance between generated holes and PEDOT:PSS occurring in rough blends could weaken the dependence of hole collection on the external field and thus explain the FF improvement of the respective devices. An additional direct evidence for the inferior transport properties of the Au:TOAB NP-based blends compared to those incorporating surfactant-free and Au:P3HT NPs is provided by time-resolved PL (TRPL) spectroscopy. TRPL measurements are widely used to determine the exciton lifetime and in our case could provide insight into the dynamics of the photogenerated excitons.[36,37] Figure 6 displays the PL intensity decay profiles obtained for the different blends onto PEDOT:PSS layers. The PL decay data were adequately fitted using a double exponential function (see the Methods section), and the associated fitting parameters are listed in Table S1 (Supporting Information). The corresponding effective exciton lifetimes, τ_{exc}, were calculated to be 140, 116, 132, and 293 ps for the reference, Au:P3HT, bare Au, and Au:TOAB-based blends, respectively. The exponential fitting of the PL decay can provide insight on the time scale of the excitons' dissociation into charge pairs within the blend.[38] Accordingly, the almost 2 times slower decay time measured in Au:TOAB-based blends can be attributed to a deficient exciton dissociation and thus charge separation. This qualitatively suggests that in this blend the fullerene regions may not be in close proximity to the polymer and that excitons need to diffuse for a longer time to reach a donor/acceptor interface compared to the blend with Au:P3HT NPs.[38] The TRPL results above further support the inhibition of the charge transfer process due to the inferior morphology of the Au:TOAB-based blend.

To better evaluate the P3HT structure in the different blends, grazing incidence XRD experiments were carried out, and Figure 7 shows the respective spectra (100) diffraction peaks corresponding to the spacing among P3HT lamellae.[39] The relative degree of P3HT crystallinity and the domain size of the different blends can be obtained by fitting the diffraction peaks and subsequently calculating the respective intensity, area, and the full width at half-maximum (fwhm). Compared to the reference blend, it is clear that the peak intensity and area

DOI: 10.1021/acsphotonics.5b00202
ACS Photonics 2015, 2, 714−723

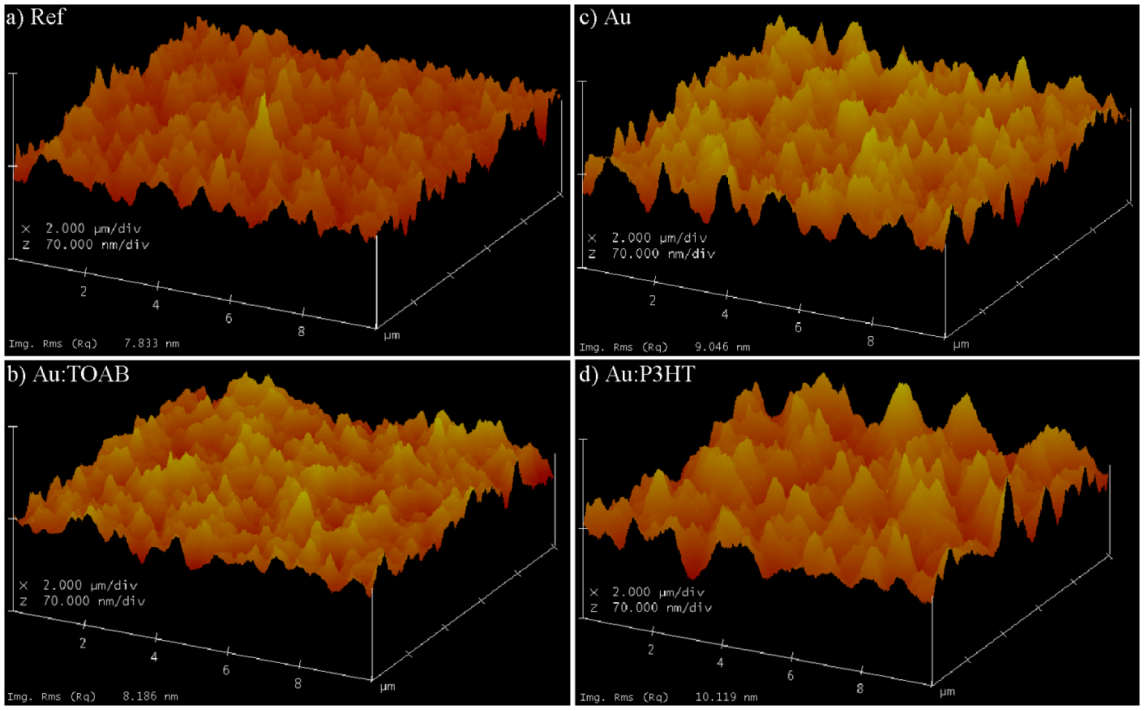

Figure 5. AFM images of the reference (a), bare NP-doped (b), Au:TOAB NP-doped (c), and Au:P3HT NP-doped (d) P3HT:PCBM BHJ layers. The rms roughness of the respective surfaces is indicated.

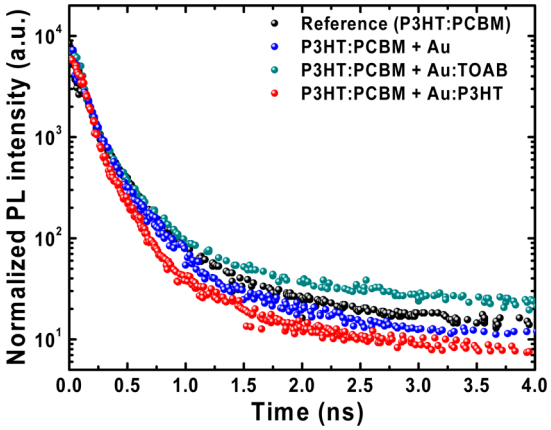

Figure 6. TRPL decay profiles for the reference (P3HT:PCBM) and plasmonic blends incorporating Au NPs terminated with different ligands.

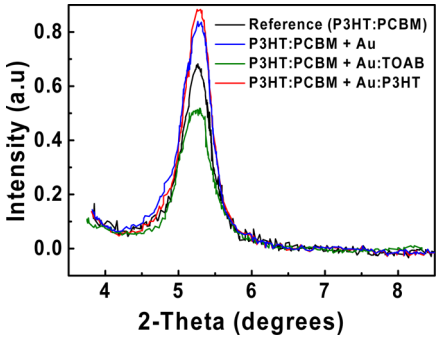

Figure 7. P3HT (100) X-ray diffraction peak measured for the reference, bare NP-doped, Au:TOAB NP-doped, and Au:P3HT NP-doped P3HT:PCBM BHJ blends.

for the Au:P3HT- and bare Au NP-doped blends increases, while its fwhm decreases, indicating that these blends exhibit a higher degree of crystallinity and ordering of the P3HT chains. On the contrary, both peak intensity and area for the Au:TOAB-doped blend remarkably decrease, indicating the inferior crystallinity of this blend. The relative fwhm's as calculated from the peaks are 0.86, 0.90, 0.92, and 1.02 for Au:P3HT, bare Au, reference, and Au:TOAB-based blends, respectively. Therefore, according to the Debye−Scherrer relationship, the P3HT domain size in the Au:P3HT-doped blend is the largest. It can be concluded that the XRD results are in accordance with the AFM and TRPL analysis and further support our observations for the transport properties of the respective blends.

As a final investigation of the effect of NPs' ligand shell on blend morphology, the resonance Raman spectra of the C═C stretching mode of P3HT in the different plasmonic BHJ blends were recorded. Figure 8a−d present the respective spectra, showing two bands around 1450 and 1470 cm^{-1} assigned to the C═C stretching modes of aggregated ($C═C_{agg}$) and unaggregated ($C═C_{un}$) P3HT components, respectively.[40,41] Aggregated species correspond to P3HT chains possessing high intra- and interchain order and long conjugation lengths, whereas unaggregated species have less intra- and interchain order and shorter conjugation lengths. The data of Figure 6 indicate that, compared to the pristine blend, the aggregated P3HT chains in the best-performing Au- and Au:P3HT-doped BHJ layers are increased at the expense of unaggregated ones (Figure 7c and d). This is in contrast to what is measured in Au:TOAB-doped blends (Figure 7b), showing a remarkable increase of $C═C_{un}$ components and thus of P3HT disorder. These results suggest the NP ligand greatly influences the P3HT chain order and in series the BHJ blend morphology in a manner that complies with the electrical performance of the respective devices. Although the above

DOI: 10.1021/acsphotonics.5b00202
ACS Photonics 2015, 2, 714−723

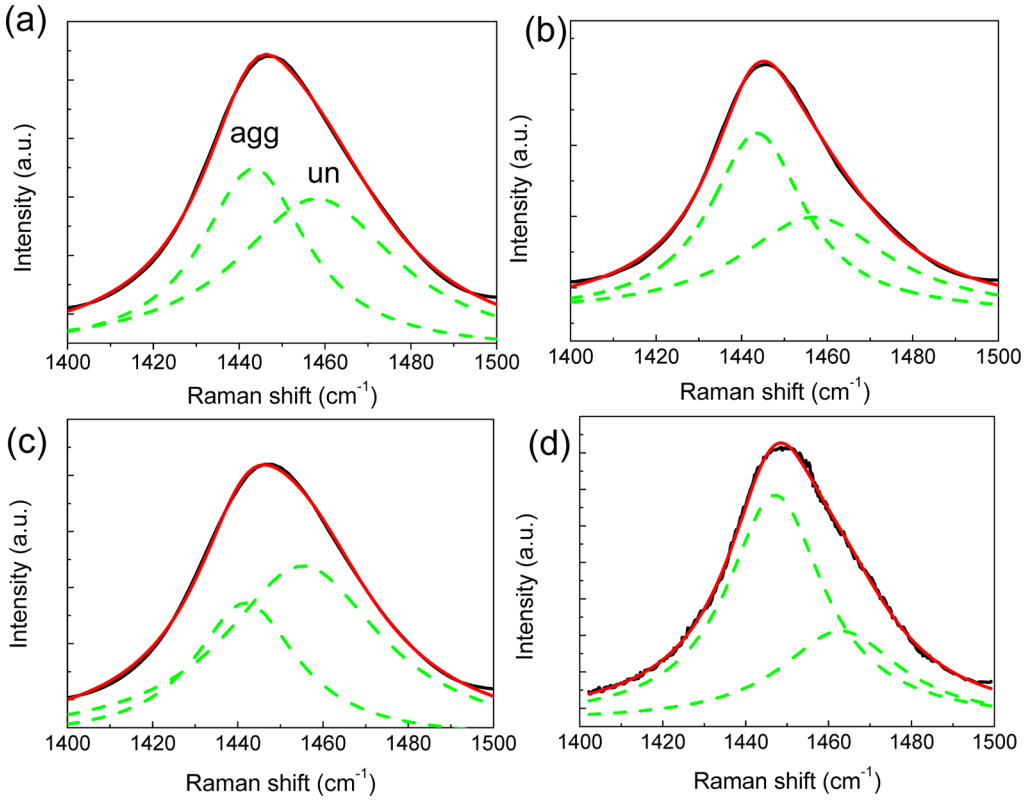

Figure 8. Resonance Raman spectra of C═C stretching modes of P3HT measured for the reference (a), bare NP-doped (b), Au:TOAB NP-doped (c), and Au:P3HT NP-doped (d) P3HT:PCBM BHJ blends. The C═C mode is fitted with two Lorentzian functions (dashed traces) of the form showing the relative contributions of both aggregated (agg) and unaggregated (un) components (see text for details).

Table 2. Photovoltaic Characteristics of Solar Cells of the Configuration ITO/PEDOT:PSS/P3HT:ICBA/Ca/Al, Incorporating Different Types of Au NPs into the Photoactive P3HT:ICBA Layer

active layer	J_{sc} (mA/cm^2)	V_{oc} (V)	FF (%)	PCE (%)
P3HT:ICBA	10.48 ± 0.18	0.84 ± 0.01	65.78 ± 0.23	5.79 ± 0.20
P3HT:ICBA + Au	11.56 ± 0.24	0.84 ± 0.01	68.83 ± 0.31	6.68 ± 0.25
P3HT:ICBA + Au:TOAB	10.25 ± 0.19	0.79 ± 0.02	56.93 ± 0.25	4.61 ± 0.23
P3HT:ICBA + Au:P3HT	12.06 ± 0.27	0.83 ± 0.01	71.51 ± 0.34	7.16 ± 0.28

results indicate that NP ligands strongly affect the blend structure, the detailed evolution of the BHJ morphology with addition of NPs is a complex problem and beyond the scope of this work.

Our results above suggest that decreasing the distance of the NPs' metallic core from the active layer polymer components, as occurs in the cases of bare and Au:P3HT NPs, appears to be an efficient way to suppress disruption of the active layer morphology and thus recombination pathways via NP-induced subgap traps.[19,42] Further confirmation on these observations was provided by two additional experimental findings. First, the performance was gradually decreased upon incorporation of laser-synthesized bare Au NPs initially terminated with a TOAB surfactant layer (Figure S3, Supporting Information). Moreover, the dispersion of the same quantity of TOAB molecules in the reference blend had no influence on its photovoltaic performance.

To further account for the validity of the above findings, we have tested the influence of the NPs' ligand shell on the performance of high-efficiency OPV cells incorporating the P3HT:ICBA photoactive layer. Figure 3b shows the respective $J-V$ curves, while Table 2 the averaged photovoltaic parameters of reference and NP-based P3HT:ICBA OPV cells, doped with the same NP types used in the case of P3HT:PCBM cells. In accordance with the case of the P3HT:PCBM system, incorporation of Au:P3HT NPs into the P3HT:ICBA photoactive layer gives rise to the best performance, leading to 23.7% PCE enhancement compared to the reference device, while devices doped with bare Au NPs showed a 15.4% PCE increase. On the contrary, the Au:TOAB-doped devices exhibited inferior performance. As also shown in Figure 4c, the above trend is followed by the respective IPCE measurements as well. The above results further support our findings on the effect of NP ligand coating on the performance of NPs-based BHJ OPV cells. Although the exact mechanisms behind the observed influence on the P3HT:ICBA system were not as thoroughly explored as in the case of the P3HT:PCBM one, it is highly possible that the situation is similar in both BHJ systems. In light of these results, further studies are in progress to fully understand and control the nature of the NPs' ligand-induced damping and loss mechanisms.

CONCLUSION

In summary, we have revealed the strong impact of NP ligand shell on the performance of plasmonic BHJ organic solar cells.

DOI: 10.1021/acsphotonics.5b00202
ACS Photonics 2015, 2, 714−723

In particular, we identified that for our OPV systems improved PCE can be obtained only when the NPs' metallic core is in direct contact with the active layer polymeric components. In particular, it is found that the effect of the NPs' coating is twofold. A minor effect is that the ligand group may act as an optical spacer between the NPs and polymer absorber, giving rise to a decreased plasmon optical field. The major effect, however, is that the morphology of the BHJ blend and in series the OPV performance are substantially influenced by the NPs' terminating coating. We envisage that this work brings about a new thinking and practices in the effort to maximize PCE via plasmonic-nanostructure-mediated light-harvesting effects.

METHODS

Laser-Assisted Synthesis of Bare Au NPs. Plasmonic Au NPs were generated by ultrafast laser ablation of a Au metallic target (99.99%) immersed in ethanol. This physical synthetic method provides the possibility of generating a large variety of NPs that are free of both surface-active substances and counterions.[21] Two steps were followed for the NP generation;[43] in the first step high laser energies were used for the production of colloids of wide size distribution. In the second step the initial colloidal solution was illuminated by a focused femtosecond laser beam. During this process, the fragmented species recoalesce to form less dispersed and much more stable NPs in the solution.[43] The NP sizes ranged from 3 to 14 nm with ~80% of the NPs exhibiting sizes between 6 and 9 nm. The morphology of NPs was characterized with high resolution transmission electron microscopy (HRTEM). The corresponding absorption spectra were measured using a PerkinElmer UV−vis spectrophotometer.

Synthesis of TOAB-Stabilized and P3HT-Functionalized Au Nanoparticles. Au nanoparticles stabilized with tetraoctylammonium bromide were prepared in a water/toluene two-phase system, using a slightly modified protocol from that described by Brust et al.[25] In detail, an aqueous solution of hydrogen tetrachloroaurate (3 mL, 30 mM) was mixed with a solution of TOAB (8 mL, 50 mM) in toluene and stirred until the tetrachloroaurate was transferred into the organic phase. The phase transfer was confirmed visually by the disappearance of the pale yellow color of the aqueous phase and the appearance of the reddish-orange color of the organic phase. Then, a freshly prepared aqueous solution of sodium borohydride (2.5 mL, 0.4 M) was slowly added while stirring vigorously and the mixture was stirred for 20 min. The ruby-colored organic phase was separated from the aqueous phase with a separating funnel and washed once with dilute sulfuric acid (20 mL, 0.1 M), twice with sodium carbonate solution (20 mL, 1 M), and finally once with water (20 mL). The organic phase was then dried over anhydrous sodium sulfate.

For the functionalization of TOAB-coated gold nanoparticles with P3HT, a freshly prepared solution of P3HT (100 μL, 4.16 mg/mL) in chloroform was added to 1 mL of TOAB-stabilized gold nanoparticles and 500 μL of toluene. The nanoparticle solution was stirred for 1 h and stored at room temperature. It is well reported that TOAB does not bind to the Au surface particularly strongly.[44] The weak binding of TOAB on the Au surface makes it convenient to exchange ligands with other capping agents.[45] In our case the sulfur groups present in the P3HT chains bind covalently to the Au surface, replacing the electrostatically bound TOAB molecules. As the sulfur groups bind to the Au surface strongly, the Au nanoparticles remain stable after ligand exchange. The morphology of P3HT-coated NPs was characterized by transmission electron microscopy by TEM (FEI Technai12) and UV−vis spectroscopy (Cary 300 Bio).

Photovoltaic Device Fabrication and Characterization. The photovoltaic devices were fabricated by spin-coating an active solution of regioregular P3HT:$PC_{60}BM$ and P3HT:$IC_{60}BA$ in 1:1 wt/wt ratio dissolved in dichlorobenzene (DCB). P3HT was purchased from Rieke Metals PCBM from Nano-C and Sollene B.V. The devices were fabricated on 20 mm × 15 mm indium−tin-oxide (ITO) glass substrates with a sheet resistance of 8−12 Ω/sq. As a hole transport layer, poly(ethylenedioxythiophene) doped with poly(4-styrenesulfonate) (PEDOT:PSS) (Clevios P VP AI 4083, Heraeus) spin-cast from an aqueous solution on the ITO substrate was used, giving an average thickness of 30 nm layer (surface resistance <80 Ω/sq), followed by 15 min baking at 120 °C. The photoactive layer was subsequently deposited by spin-coating the P3HT:fullerene:NPs blend at 1000 rpm. Subsequently, 100 nm Al (at a constant rate of 1.5 A/s) or bilayer 100 nm Al/20 nm Ca (at a constant rate of 1.5 A/s for Al and 0.2 A/s for Ca) cathodes were thermally evaporated through a shadow mask and completed the whole stack of solar cells. Finally, a postfabrication annealing was performed at 150 °C for 15 min inside a glovebox (<0.1 ppm O_2) under a nitrogen atmosphere for both cases.

All types of NP dispersions were mixed in the active BHJ solutions in vol/vol ratios. In particular, reference solutions of the different types of NPs used (bare, stabilized with TOAB and with P3HT ligands) were prepared to exhibit identical optical densities at the characteristic plasmon resonance wavelength. Subsequently, the active layers were realized by mixing respective solutions of P3HT and fullerene derivatives at 1:1 ratio and Au NPs in DCB. The corresponding volume ratios of the P3HT:fullerene and the Au NP solutions ranged from 3% to 6%. It should be noted here that the excess P3HT used to terminate the Au:P3HT NPs was taken into account during the preparation of the respective P3HT:fullerene-Au:P3HT solutions. Prior to spin-coating onto PEDOT:PSS/ITO substrates, the mixtures were stirred in a controlled glovebox environment for 24 h at 55 °C in order to remove the initial NP solvent from DCB. In all cases, the final active layer thickness, determined from cross-sectional SEM images (not shown), is measured to be 165 ± 5 nm. Detailed information on the optimized fabrication and characterization conditions for the pristine ITO/PEDOT:PSS/P3HT:PCBM/Al can be found elsewhere.[14]

The performances of the devices were measured at room temperature with an Air Mass 1.5 Global (AM 1.5 G) solar simulator at an intensity of 100 mW/cm^2. A reference monocrystalline silicon solar cell from Newport was used to calibrate the lamp. All measurements were made in air immediately after device fabrication. The external quantum efficiency measurements were conducted immediately after device fabrication without any encapsulation process in ambient conditions using an integrated system (Enlitech, Taiwan) and a lock-in amplifier with a current preamplifier under short-circuit conditions. In all cases, the best devices are attained for an NP/BHJ blend volume ratio of 5%, and only results from such optimized devices are demonstrated here.

Hole-only devices with the structure ITO/PEDOT:PSS/P3HT:PCBM(NPs)/Au were additionally fabricated for all the different types of devices. The hole mobility was estimated

DOI: 10.1021/acsphotonics.5b00202
ACS Photonics 2015, 2, 714−723

from the $J-V$ characteristics in the low-voltage region, where the current is described by the Mott–Gurney square law:

$$J_{SCLC} = \frac{9}{8}\varepsilon_o\varepsilon_r\mu_h\frac{V^2}{L^3} \quad (1)$$

where ε_o is the permittivity of free space, ε_r is the dielectric constant of the active layer, μ_h is the hole mobility, and L is the active layer film thickness.

Characterization of the Bulk Heterojunction Blends. UV–vis absorption spectra were recorded using a PerkinElmer (Lambda 950) spectrophotometer. The morphology of the blend surfaces was examined by tapping-mode atomic force microscopy (Digital Instruments NanoScope IIIa). For the PL measurements the devices were placed into a vacuum chamber with optical access. For sample excitation a He–Cd CW laser operating at a wavelength of 325 nm, with 35 mW power, is used. The PL spectra were measured at room temperature and resolved by using a UV grating and a sensitive, calibrated liquid nitrogen cooled CCD camera. For the TRPL measurements, the samples were excited using a 515 nm picosecond laser (Light Conversion Pharos system); the dynamic signal was recorded using time-correlated single-photon-counting spectroscopy. The system exhibited a time-resolution of 50 ps after deconvolution with the spectrometer response function. The PL decay data were adequately fitted using a double-exponential function of the form

$$I(t) = I_1e^{-t/\tau 1} + I_2e^{-t/\tau 2} \quad (2)$$

where $I_{1,2}$ are the amplitudes of the decay and $\tau_{1,2}$ are the corresponding exponential constants. The contribution of each of the two time constants is quantified by its relative amplitude, $A_{1,2}$, expressed as

$$A_{1,2} = \frac{I_{1,2}}{I_1 + I_2} \times 100\%$$

To obtain a quantitative measure of the charge transfer process, an effective exciton lifetime is defined in the blends as $\tau_{exc} = A_1\tau_1 + A_2\tau_2$. The resonance Raman spectra of the blends were recorded using a micro-Raman spectrometer (Nicolet Almega XR); a 473 nm laser was used as the excitation source. The structure and crystallinity of the different blends were determined by grazing incidence X-ray diffraction using a Rigaku diffractometer with Cu Kα radiation. The incident X-ray angle was set to 2.5°.

■ ASSOCIATED CONTENT

Supporting Information

We show typical TEM images and respective size distributions of chemically and laser-synthesized nanoparticles, $J-V$ characteristics of NP-based ITO/PEDOT:PSS/P3HT:PCBM/Ca/Al devices and of devices incorporating laser-synthesized bare Au NPs initially terminated with a TOAB surfactant layer. Furthermore, we present TRPL decay fitting parameters and photovoltaic characteristics of solar cells of the configuration ITO/PEDOT:PSS/P3HT:PCBM/Ca/Al, incorporating different types of Au NPs into the photoactive P3HT:PCBM layer. The Supporting Information is available free of charge on the ACS Publications website at DOI: 10.1021/acsphotonics.5b00202.

■ AUTHOR INFORMATION

Corresponding Author

*E-mail: stratak@iesl.forth.gr.

Notes

The authors declare no competing financial interest.

■ ACKNOWLEDGMENTS

The authors acknowledge Ms. A. Manousaki for her support with the atomic force microscope. This research has been financially supported by the Penelope (3116) Project, which is implemented under the ARISTEIA II Action of the "Operational Programme Education and Life-long Learning" and is cofunded by the European Social Fund (ESF) and National Resources. The authors would also like to thank the EU COST action MP1202 "Rational design of hybrid organic-inorganic interfaces: the next step towards advanced functional material" for collaboration opportunities.

■ REFERENCES

(1) You, J.; Dou, L.; Yoshimura, K.; Kato, T.; Ohya, K.; Moriarty, T.; Emery, K.; Chen, C.-C.; Gao, J.; Li, G. A polymer tandem solar cell with 10.6% power conversion efficiency. *Nat. Commun.* **2013**, *4*, 1446.

(2) He, Z.; Zhong, C.; Su, S.; Xu, M.; Wu, H.; Cao, Y. Enhanced power-conversion efficiency in polymer solar cells using an inverted device structure. *Nat. Photonics* **2012**, *6*, 591.

(3) Gaudiana, R.; Brabec, C. J. Organic materials: fantastic plastic. *Nat. Photonics* **2008**, *2*, 287.

(4) E.P.I. Association, Global Market Outlook for Photovoltaics 2013–2017,http://www.epia.org/fileadmin/user_upload/Publications/GMO_2013_-_Final_PDF.pdf.

(5) Abdulrazzaq, O. A.; Saini, V.; Bourdo, S.; Dervishi, E.; Biris, A. S. Organic solar cells: a review of materials, limitations, and possibilities for improvement. *Part. Sci. Technol.* **2013**, *31*, 427.

(6) Reese, M. O.; Nardes, A. M.; Rupert, B. L.; Larsen, R. E.; Olson, D. C.; Lloyd, M. T.; Shaheen, S. E.; Ginley, D. S.; Rumbles, G.; Kopidakis, N. Photoinduced degradation of polymer and polymer–fullerene active layers: experiment and theory. *Adv. Funct. Mater.* **2010**, *20*, 3476.

(7) Dennler, G.; Scharber, M. C.; Brabec, C. J. Polymer-fullerene bulk-heterojunction solar cells. *Adv. Mater.* **2009**, *21*, 1323.

(8) Stratakis, E.; Kymakis, E. Nanoparticle-based plasmonic organic photovoltaic devices. *Mater. Today* **2013**, *16*, 133.

(9) Gan, Q.; Bartoli, F. J.; Kafafi, Z. H. Plasmonic-enhanced organic photovoltaics: breaking the 10% efficiency barrier. *Adv. Mater.* **2013**, *25*, 2385.

(10) Atwater, H. A.; Polman, A. Plasmonics for improved photovoltaic devices. *Nat. Mater.* **2010**, *9*, 205.

(11) Su, Y.-H.; Ke, Y.-F.; Cai, S.-L.; Yao, Q.-Y. Surface plasmon resonance of layer-by-layer gold nanoparticles induced photoelectric current in environmentally-friendly plasmon-sensitized solar cell. *Light: Sci. Appl.* **2012**, *1*, e14.

(12) Wang, D. H.; Park, K. H.; Seo, J. H.; Seifter, J.; Jeon, J. H.; Kim, J. K.; Park, J. H.; Park, O. O.; Heeger, A. J. Enhanced power conversion efficiency in PCDTBT/PC70BM bulk heterojunction photovoltaic devices with embedded silver nanoparticle clusters. *Adv. Energy Mater.* **2011**, *1*, 766.

(13) Kim, C.-H.; Cha, S.-H.; Kim, S. C.; Song, M.; Lee, J.; Shin, W. S.; Moon, S.-J.; Bahng, J. H.; Kotov, N. A.; Jin, S.-H. Silver nanowire embedded in P3HT:PCBM for high-efficiency hybrid photovoltaic device applications. *ACS Nano* **2011**, *5*, 3319.

(14) Spyropoulos, G. D.; Stylianakis, M. M.; Stratakis, E.; Kymakis, E. Organic bulk heterojunction photovoltaic devices with surfactant-free Au nanoparticles embedded in the active layer. *Appl. Phys. Lett.* **2012**, *100*, 213904.

(15) Kakavelakis, G.; Stratakis, E.; Kymakis, E. Synergetic plasmonic effect of Al and Au nanoparticles for efficiency enhancement of air

DOI: 10.1021/acsphotonics.5b00202
ACS Photonics 2015, 2, 714–723

processed organic photovoltaic devices. *Chem. Commun.* **2014**, *50*, 5285.
(16) Kakavelakis, G.; Stratakis, E.; Kymakis, E. Aluminum nanoparticles for efficient and stable organic photovoltaics. *RSC Adv.* **2013**, *3*, 16288.
(17) Topp, K.; Borchert, H.; Johnen, F.; Tunc, A. V.; Knipper, M.; von Hauff, E.; Parisi, J.; Al-Shamery, K. Impact of the incorporation of Au nanoparticles into polymer/fullerene solar cells. *J. Phys. Chem. A* **2009**, *114*, 3981.
(18) Xue, M.; Li, L.; de Villers, B. J. T.; Shen, H.; Zhu, J.; Yu, Z.; Stieg, A. Z.; Pei, Q.; Schwartz, B. J.; Wang, K. L. Charge-carrier dynamics in hybrid plasmonic organic solar cells with Ag nanoparticles. *Appl. Phys. Lett.* **2011**, *98*, 253302.
(19) Wu, B.; Wu, X.; Guan, C.; Tai, K. F.; Yeow, E. K. L.; Fan, H. J.; Mathews, N.; Sum, T. C. Uncovering loss mechanisms in silver nanoparticle-blended plasmonic organic solar cells. *Nat. Commun.* **2013**, *4*, 2004.
(20) Stratakis, E.; Barberoglou, M.; Fotakis, C.; Viau, G.; Garcia, C.; Shafeev, G. A. Generation of Al nanoparticles via ablation of bulk Al in liquids with short laser pulses. *Opt. Express* **2009**, *17*, 12650.
(21) Yang, G. *Laser Ablation in Liquids: Principles and Applications in the Preparation of Nanomaterials*; CRC Press: Boca Raton, FL, 2012.
(22) Paci, B.; Spyropoulos, G. D.; Generosi, A.; Bailo, D.; Albertini, V. R.; Stratakis, E.; Kymakis, E. Enhanced Structural Stability and Performance Durability of Bulk Heterojunction Photovoltaic Devices Incorporating Metallic Nanoparticles. *Adv. Funct. Mater.* **2011**, *21*, 3573.
(23) Liao, H.-C.; Tsao, C.-S.; Lin, T.-H.; Jao, M.-H.; Chuang, C.-M.; Chang, S.-Y.; Huang, Y.-C.; Shao, Y.-T.; Chen, C.-Y.; Su, C.-J.; Jeng, U. S.; Chen, Y.-F.; Su, W.-F. Nanoparticle-tuned self-organization of a bulk heterojunction hybrid solar cell with enhanced performance. *ACS Nano* **2012**, *6*, 1657.
(24) Zhao, G.; He, Y.; Li, Y. 6.5% Efficiency of Polymer Solar Cells Based on Poly(3-hexylthiophene) and Indene-C_{60} Bisadduct by Device Optimization. *Adv. Mater.* **2010**, *22*, 4355.
(25) Brust, M.; Walker, M.; Bethell, D.; Schiffrin, D. J.; Whyman, R. Synthesis of thiol derivatised gold nanoparticles in a two-phase liquid/liquid system. *J. Chem. Soc., Chem. Commun.* **1994**, 801.
(26) Shen, H.; Bienstman, P.; Maes, B. Plasmonic absorption enhancement in organic solar cells with thin active layers. *J. Appl. Phys.* **2009**, *106*, 073109.
(27) Catchpole, K. R.; Polman, A. Plasmonic solar cells. *Opt. Express* **2008**, *16*, 21793.
(28) Lee, W. H.; Chuang, S. Y.; Chen, H. L.; Su, W. F.; Lin, C. H. Exploiting optical properties of P3HT:PCBM films for organic solar cells with semitransparent anode. *Thin Solid Films* **2010**, *518*, 7450.
(29) Kelly, K. L.; Coronado, E.; Zhao, L. L.; Schatz, G. C. The optical properties of metal nanoparticles: the influence of size, shape, and dielectric environment. *J. Phys. Chem. B* **2003**, *107*, 668.
(30) Atwater, A.; Polman, A. Plasmonics for improved photovoltaic devices. *Nat. Mater.* **2010**, *9*, 205.
(31) Lee, J. H.; Park, J. H.; Kim, J. S.; Lee, D. Y.; Cho, K. High efficiency polymer solar cells with wet deposited plasmonic gold nanodots. *Org. Electron.* **2009**, *10*, 416.
(32) Paci, B.; Generosi, A.; Albertini, V. R.; Spyropoulos, G. D.; Stratakis, E.; Kymakis, E. Enhancement of photo/thermal stability of organic bulk heterojunction photovoltaic devices via gold nanoparticles doping of the active layer. *Nanoscale* **2012**, *4*, 7452.
(33) Paci, B.; Bailo, D.; Albertini, V. R.; Wright, J.; Ferrero, C.; Spyropoulos, G.; Stratakis, E.; Kymakis, E. Spatially-resolved in-situ Structural Study of Organic Electronic Devices with Nanoscale Resolution: The Plasmonic Photovoltaics Case Study. *Adv. Mater.* **2013**, *25*, 4760.
(34) Li, G.; Shrotriya, V.; Yao, Y.; Yang, Y. Polymer self-organization enhances photovoltaic efficiency. *J. Appl. Phys.* **2005**, *98*, 043704.
(35) Hsu, M.-H.; Yu, P.; Huang, J.-H.; Chang, C.-H.; Wu, C.-W.; Cheng, Y.-C.; Chu, C.-W. Balanced carrier transport in organic solar cells employing embedded indium-tin-oxide nanoelectrodes. *Appl. Phys. Lett.* **2011**, *98*, 073308.
(36) Huang, J. H.; Chien, F. C.; Chen, P. L.; Ho, K. C.; Chu, C. W. Monitoring the 3D nanostructures of bulk heterojunction polymer solar cells using confocal lifetime imaging. *Anal. Chem.* **2010**, *82*, 1669.
(37) Wu, J.-L.; Chen, F.-C.; Hsiao, Y.-S.; Chien, F.-C.; Chen, P.; Kuo, C.-H.; Huang, M. H.; Hsu, C.-S. Surface plasmonic effects of metallic nanoparticles on the performance of polymer bulk heterojunction solar cells. *ACS Nano* **2011**, *5*, 959.
(38) Hedley, G. J.; Ward, A. J.; Alekseev, A.; Howells, C. T.; Martins, E. R.; Serrano, L. A.; Cooke, G.; Ruseckas, A.; Samuel, I. D. W. Determining the optimum morphology in high-performance polymer-fullerene organic photovoltaic cells. *Nat. Commun.* **2013**, *4*, 2867.
(39) Sirringhaus, H.; Brown, P. J.; Friend, R. H.; Nielsen, M. M.; Bechgaard, K.; Langeveld-Voss, B. M. W.; Spiering, A. J. H.; Janssen, R. A. J.; Meijer, E. W.; Herwig, P.; de Leeuw, D. M. Two-dimensional charge transport in self-organized, high-mobility conjugated polymers. *Nature* **1999**, *401*, 685.
(40) Gao, Y.; Grey, J. K. Resonance chemical imaging of polythiophene/fullerene photovoltaic thin films: mapping morphology-dependent aggregated and unaggregated C═C species. *J. Am. Chem. Soc.* **2009**, *131*, 9654.
(41) Tsoi, W. C.; James, D. T.; Kim, J. S.; Nicholson, P. G.; Murphy, C. E.; Bradley, D. D. C.; Nelson, J.; Kim, J. The nature of in-plane skeleton Raman modes of P3HT and their correlation to the degree of molecular order in P3HT:PCBM blend thin films. *J. Am. Chem. Soc.* **2011**, *133*, 9834.
(42) Wang, C. C. D.; Choy, W. C. H.; Duan, C.; Fung, D. D. S.; Sha, W. E. I.; Xie, F.-X.; Huang, F.; Cao, Y. Optical and electrical effects of gold nanoparticles in the active layer of polymer solar cells. *J. Mater. Chem.* **2012**, *22*, 1206.
(43) Besner, S.; Kabashin, A.; Meunier, M. *Appl. Phys. Lett.* **2006**, *89*, 233122.
(44) Thomas, K. G.; Zajicek, J.; Kamat, P. V. Surface binding properties of tetraoctylammonium bromide-capped gold nanoparticles. *Langmuir* **2002**, *18*, 3722.
(45) Lu, Z.; Goebl, J.; Ge, J.; Yin, Y. Self-assembly and tunable plasmonic property of gold nanoparticles on mercapto-silica microspheres. *J. Mater. Chem.* **2009**, *19*, 4597.

DOI: 10.1021/acsphotonics.5b00202
ACS Photonics 2015, 2, 714−723